(Received 26 October 2023, Accepted 7 December 2023, Scheduled 17 December 2023)

An X-Band Frequency Beam-Scanning Circularly-Polarized Leaky-Wave Antenna with Low Axial Ratio in All Half-Power Beamwidth Ranges

Dezhuang Zhang[1], Zhongbao Wang[1,2,*], Zhixia Xu[1], Hongmei Liu[1], Mingming Gao[1,2], and Shaojun Fang[1]

[1] *School of Information Science and Technology, Dalian Maritime University, Dalian, Liaoning 116026, China*
[2] *Liaoning Key Laboratory of Radio Frequency and Big Data for Intelligent Applications, Liaoning Technical University Huludao, Liaoning 125105, China*

ABSTRACT: A novel frequency beam-scanning circularly-polarized leaky-wave antenna with the axial ratio (AR) of less than 3 dB in all the half-power beamwidth ranges based on an H-shaped slow-wave transmission line is proposed for X-band applications. The proposed circularly-polarized leaky-wave antenna is composed of a novel slow-wave transmission line and two rows of elliptical patch structures, leading to wide AR bandwidth, backward-to-forward beam scanning, and stable gain. To verify the proposed antenna, one prototype with a center frequency of 10 GHz is designed and fabricated. Measured results indicate that the main beam scans from -25° to $+28^\circ$ within the operating frequency variation from 8.7 to 11.5 GHz. The 3-dB AR bandwidth and maximum gain are 27.7% and 10.28 dBic, respectively.

1. INTRODUCTION

Leaky-wave antennas (LWAs) have received widespread attention due to their characteristics of beam scanning with frequency, simple feed structure, high gain, and low profile in recent years [1], which may be widely used in indoor communication, wireless communication, and satellite system [2]. Nowadays, most LWAs are proposed based on various structures, including rectangle waveguides [3], substrate integrated waveguides [4], composite right-/left-handed [5], Goubau line [6], and microstrip line [7]. However, conventional LWAs mainly have linear polarization, and due to the presence of metal ground, the radiation efficiency is low.

Circularly polarized (CP) LWAs based on slow-wave transmission lines have attracted much attention due to their low attenuation in rainy and snowy weather and strong ability to penetrate the ionosphere. A double-layer LWA using a slow-wave transmission structure with loaded metal via holes has been reported in [8], which realizes 3-dB axial ratio (AR) bandwidth of 15%. In [9], periodic elements were designed on the top layer to achieve CP beam scanning characteristics, and the antenna was fed by a slow-wave transmission line on the bottom substrate. However, the presence of vias and multi-layer structures results in low antenna integration, limiting the application of LWAs. Besides, a reconfigurable LWA was designed in [10], which achieved switchable right/left-hand CP and linearly polarized radiation functions by controlling two PIN diodes. In [11], a continuous 35° CP beam scanning planar LWA was designed by using a modulated slow-wave transmission line based on a slot-line and spoof surface plasmon polariton (SSPP) structure. The LWAs in [10, 11] have forward CP beam scanning ability instead of backward-broadside-forward radiation. A CP LWA with high radiation efficiency was proposed in [12]. However, the antenna beam scanning ability is only 15° (i.e., -7° to $+8^\circ$). In [13], a CP microstrip LWA array was proposed by a series of periodic conformal radiation patches. The method of CP conformal LWA has achieved a bandwidth of 500 MHz (from 9.5 to 10 GHz) with an AR of less than 4 dB in the half-power beamwidth (HPBW) range. A herringbone CP LWA with broadside radiation was reported in [14]. However, the LWAs proposed in [13] and [14] have narrow AR bandwidth. Besides, most CP LWAs only focus on the AR at the maximum radiation direction during beam scanning with the variation of frequencies. In view of this, it is necessary to reduce the AR of LWA within HPBW, increase the AR bandwidth, and achieve beam scanning from backward to forward.

In this paper, a novel frequency beam-scanning CP LWA with an AR of less than 3 dB in all the HPBW ranges based on the H-shaped slow-wave transmission line is proposed. The proposed LWA is composed of a novel H-shaped slow-wave transmission line and two rows of elliptical patch structures. The beam scanning angle of the antenna can be effectively widened by the dispersion characteristics of the H-shaped slow-wave transmission line. Two rows of elliptical patches are used to achieve CP radiation through electromagnetic (EM) coupling with the slow-wave transmission line and reduce the AR in all HPBW ranges. A CP LWA is fabricated and measured to validate the proposed method.

* Corresponding author: Zhongbao Wang (wangzb@dlmu.edu.cn).

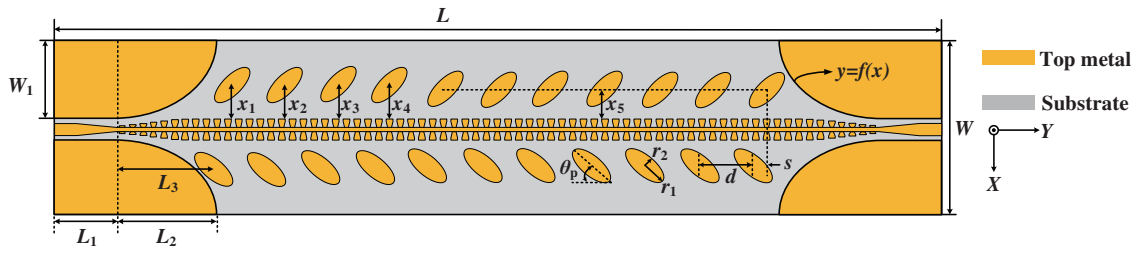

FIGURE 1. Configuration of the proposed CP LWA.

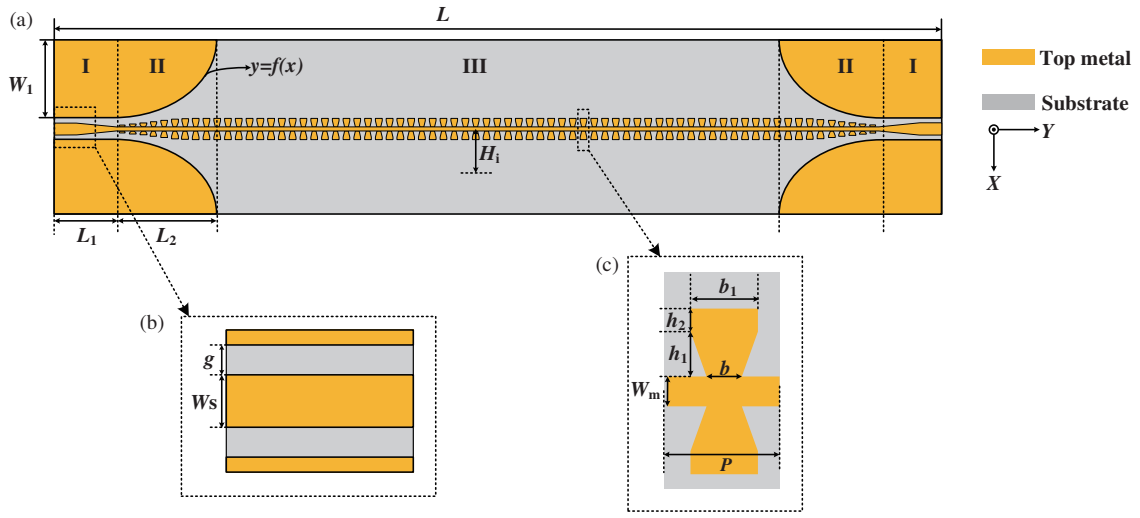

FIGURE 2. Configuration of the proposed H-shaped slow-wave transmission line. (a) Perspective view. (b) CPW. (c) Slow-wave transmission line unit.

2. ANTENNA ANALYSIS AND DESIGN

The configuration of the proposed frequency beam-scanning CP LWA is shown in Fig. 1. It can be seen that the proposed antenna consists of two sections of coplanar waveguide (CPW), mode-transition unit structures, one section of a novel H-shaped slow-wave transmission line, and two rows of elliptical patches. Groundless CPW and each of the mode-transition units can achieve a perfect transition from quasi-TEM mode to SSPP mode. The novel H-shaped slow-wave transmission line can satisfy the requirements of EM wave transmission from one port to another and achieve beam scanning from backward to forward. Elliptical patches are periodically arranged on both sides of the slow-wave transmission line, which can radiate EM waves and obtain CP characteristics.

The length and width of the proposed CP LWA are $L = 250\,\text{mm}$ and $W = 50\,\text{mm}$, respectively. It is designed on a 1.5-mm thick F4B substrate with relative dielectric constant $\varepsilon_r = 2.65$ and loss tangent $\tan\delta = 0.002$. Besides, it is obvious that the analysis of slow-wave transmission line characteristics is particularly important in the proposed antenna design. The configuration of the proposed H-shaped slow-wave transmission line is shown in Fig. 2(a). It can be seen that the proposed H-shaped slow-wave transmission line consists of Region I, Region II, and Region III. In order to achieve impedance matching between the two ports, two sections of CPW are designed in Region I, which has an input impedance of $50\,\Omega$. For the CPW transmission line at ports, the strip width, gap size, width of Region I, and length of Region I are chosen as $W_s = 3.5\,\text{mm}$, $g = 0.2\,\text{mm}$, $W_1 = 23\,\text{mm}$, and $L_1 = 17\,\text{mm}$, respectively. In addition, the matching units with seven grooves gradually increasing in depth are designed in Region II to achieve the transition from quasi-TEM mode to SSPP mode [15]. Region III is the main transmission part of the slow-wave transmission line. To accommodate single conductor slow-wave transmission line, the CPW grounding plane eventually disappears in the form of an exponential function $y = f(x) = e^{\alpha x} - 1$, where $\alpha = \ln(W_1 + 1)/L_2$ and $L_2 = 30\,\text{mm}$. The slow-wave transmission line unit used in this work is schematically shown in Fig. 2(c), whose parameters are $P = 3\,\text{mm}$, $W_m = 1\,\text{mm}$, $b = 1\,\text{mm}$, $b_1 = 2\,\text{mm}$, $h_1 = 2\,\text{mm}$, and $h_2 = 0.5\,\text{mm}$.

To explore the propagation characteristics of slow-wave transmission line, the unit cell is analyzed by the eigen-mode solver of CST Microwave studio, and the simulated results are depicted in Fig. 3. We can observe that the dispersion curve of the slow-wave transmission line unit gradually moves away from the light line and eventually reaches an asymptotic frequency, which means that the transmission structure operates in the slow-wave region and cannot radiate into free space. As shown in Fig. 3, when the groove depths h_1 and h_2 are increased respectively, the asymptotic frequency is decreased. In

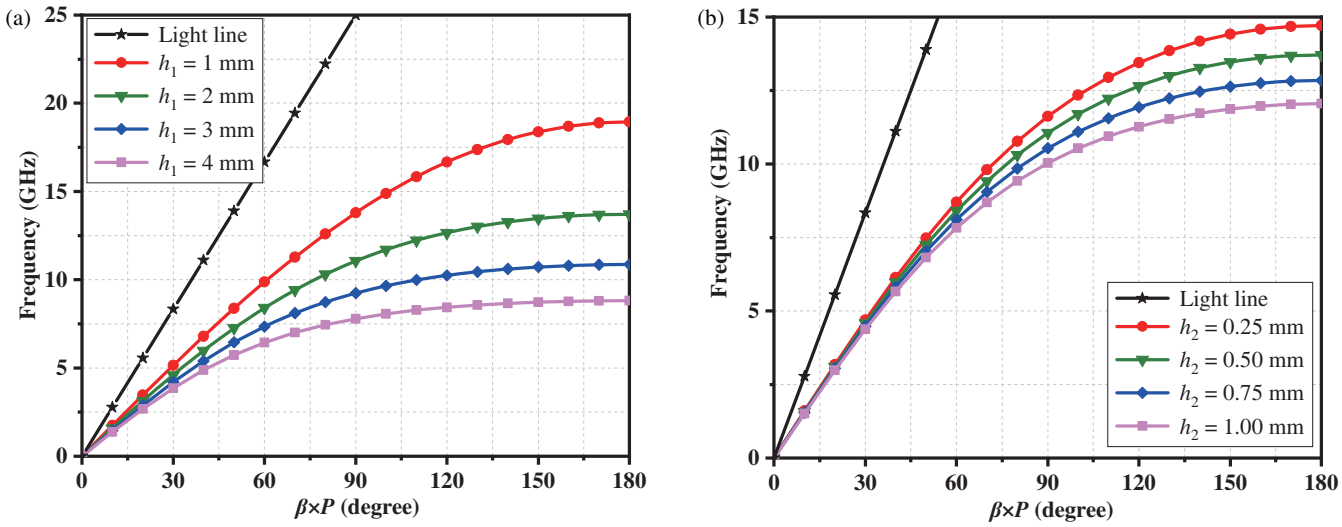

FIGURE 3. Dispersion diagrams of the slow-wave transmission line unit cell. (a) Different h_1. (b) Different h_2.

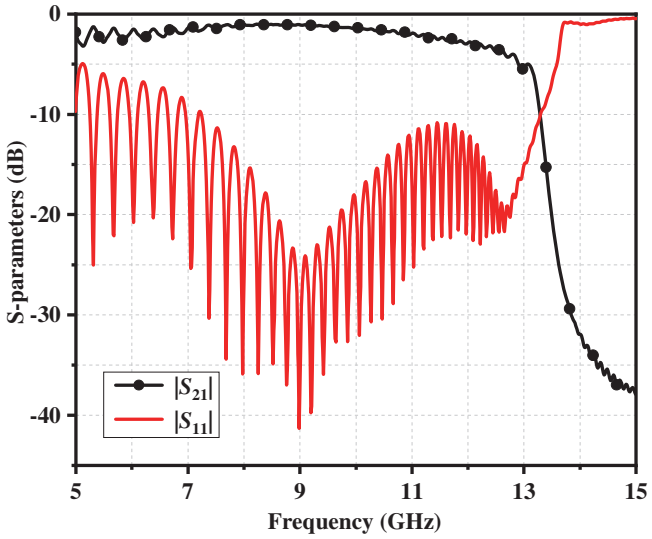

FIGURE 4. Transmission property of the proposed slow-wave transmission line.

this work, in order to ensure the good transmission characteristics of slow-wave transmission line in the X-band, h_1 is selected as 2 mm and h_2 as 0.5 mm to achieve an asymptotic frequency of 13.3 GHz.

To validate transmission property of the proposed slow-wave transmission line, simulated S-parameters and near E-field distribution are shown in Figs. 4 and 5, respectively. As shown in Fig. 4, when the frequency is less than 13.3 GHz, EM waves can be effectively transmitted from one port to another, which is consistent with the analysis results of the dispersion curve in Fig. 3(a) and the E-field distribution in Fig. 5. Besides, it is observed from Fig. 5 that EM waves at 8 and 10 GHz are tightly confined to both sides of the slow-wave transmission line, indicating that the electric field cannot radiate into free space, which is consistent with the transmission characteristics of slow-wave.

Because EM wave in slow-wave transmission line fails to propagate into free space, two rows of elliptical metal patches are used to coupling with the slow-wave transmission line and generate radiating modes. According to the Floquet theory [16], multiple spatial harmonics are excited as a result of the structure's periodicity, and their phase constants are as follows:

$$\beta_n = \beta_0 + 2n\pi/P, \quad n = 0, \pm1, \pm2, \ldots \tag{1}$$

where β_n is the n^{th} space harmonic wave number, β_0 the propagation constant of the fundamental mode of the slow-wave transmission line, and P the period of the y-directional perturbations. For a single-beam CP LWA, the $n = -1$ space harmonic is used to radiate, whose wave number is

$$\beta_{-1} = \beta_0 - 2\pi/P \tag{2}$$

This means that β_{-1} of the antenna can be changed by changing the length of period P, which is used to realize the backward-to-

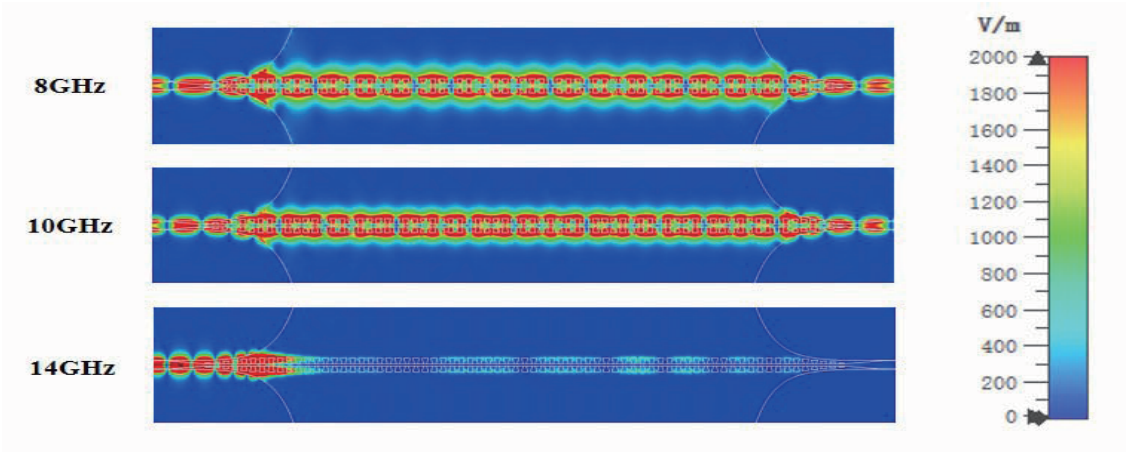

FIGURE 5. Simulated E-field distribution of the proposed slow-wave transmission line at 8, 10, and 14 GHz.

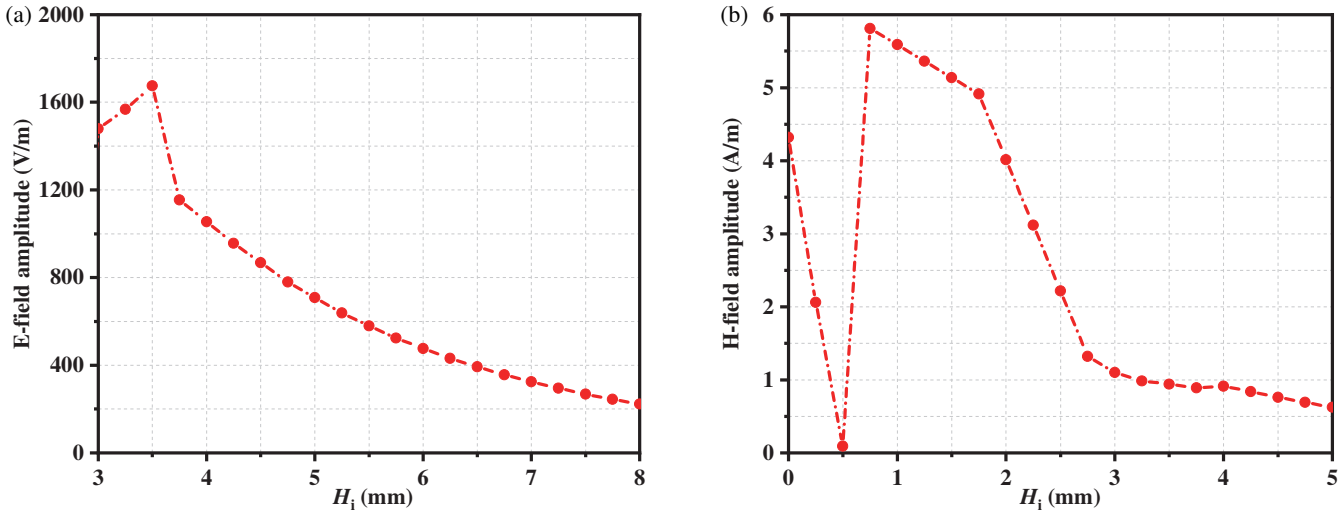

FIGURE 6. Effect of H_i on the amplitude of both E-field and H-field in the x-axis. (a) E-field. (b) H-field.

forward beam scanning of the proposed CP LWA. The direction of the main beam is determined by:

$$\theta = \arcsin(\beta_{-1}/k_0) \tag{3}$$

where k_0 is the propagation constant in free space, and θ is the angle between the beam direction and $+z$ axis.

To achieve CP radiation, the elliptical patches loaded in the upper row and lower row are offset along the y-axis direction by $s = \lambda_g/4$ (λ_g is the guided wavelength of slow-wave transmission line), and each patch rotates $\theta_p = 45°$ relative to its center, which results in a 90° phase difference between the two rows of elliptical patches and then realizes CP radiation. The distance between the center of the first elliptical radiation patch and the metal ground of CPW is $L_3 = 27$ mm. According to the dispersion curve for $h_1 = 2$ mm and $h_2 = 0.5$ mm in Fig. 3(a), at center frequency 10 GHz, $\beta \times P = 0.425\pi$, then $\lambda_g = 2\pi/\beta = 14.1$ mm. In order to achieve broadside radiation ($\theta = 0°$) at 10 GHz, the period of the elliptical patches d is selected as λ_g. After optimization with EM simulation software HFSS, the period of the elliptical patches is set to $d = 15.3$ mm, and the offset between the upper and lower elliptical patches is $s = 3.825$ mm.

Figure 6 shows the effect of H_i on the amplitude of the simulated E-field and H-field along the y-axis direction of the proposed slow-wave transmission line. When the distance H_i from slow-wave transmission line is increased from 3.5 to 8 mm or from 0.75 to 5 mm, the amplitude of the electric or magnetic field is decreased. Thus, the distance between elliptical patches and slow-wave transmission line plays an important role in electronic and magnetic coupling. Based on [17], the strength of the electric- and magnetic-field coupling between elliptical patches and slow-wave transmission line (C_J and C_M) can be calculated by:

$$C_{\mathrm{J}} = \int_v \vec{E} \cdot \vec{J} \mathrm{d}v \tag{4}$$

$$C_{\mathrm{M}} = \int_v \vec{H} \cdot \vec{M} \mathrm{d}v \tag{5}$$

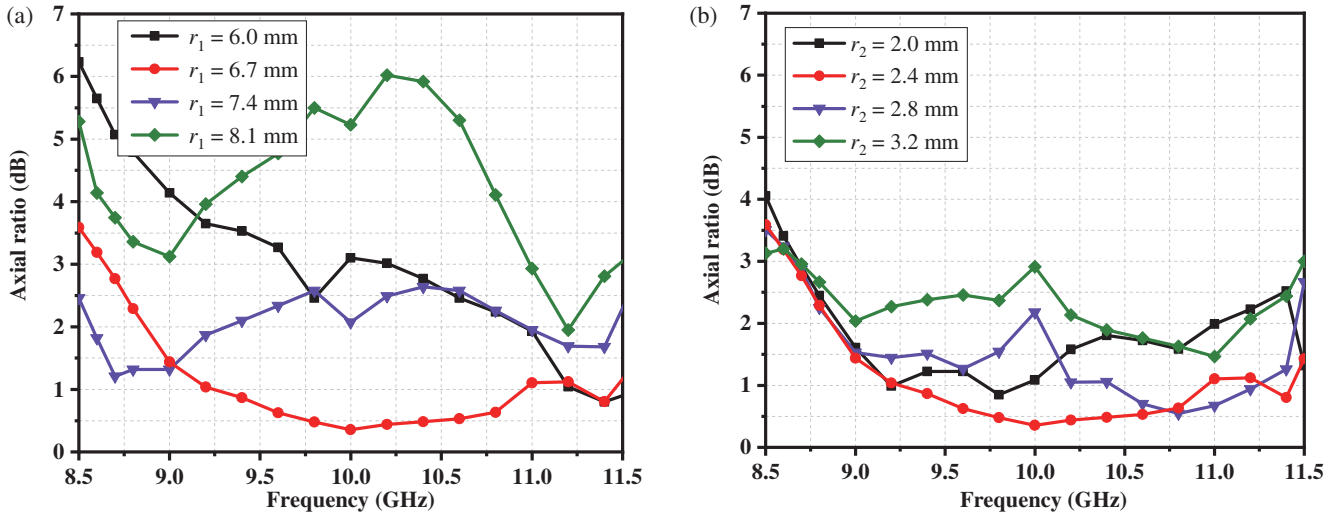

FIGURE 7. Effect of r_1 and r_2 on the AR of the proposed CP LWA. (a) r_1. (b) r_2.

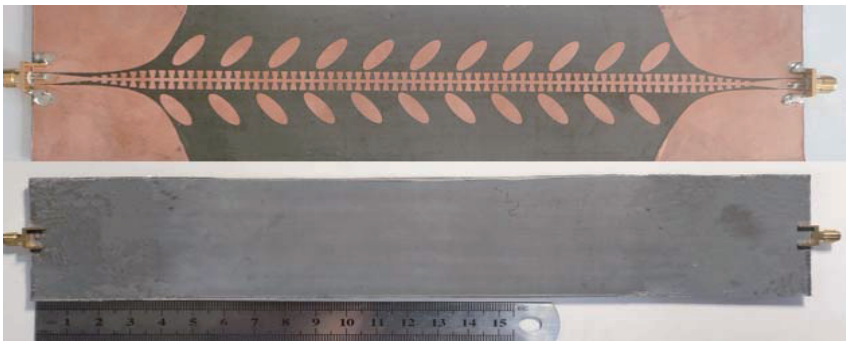

FIGURE 8. Front and bottom view of the fabricated CP LWA.

where $\vec{E}$ and $\vec{H}$ are electric- and magnetic-field intensities of the element, respectively; $\vec{J}$ and $\vec{M}$ are the equivalent electric and magnetic current densities, respectively. Equations (4) and (5) show that the coupling strength between radiation patches and slow-wave transmission line is influenced by the E-field and H-field intensities (i.e., the distance between radiation patches and slow-wave transmission line). In order to achieve an AR of less than 3 dB within all the HPBWs and reduce the side-lobe level of the proposed CP LWA, the distances between radiation patches and slow-wave transmission line are adjusted as follows: $x_1 = 6.75$ mm, $x_2 = 6.55$ mm, $x_3 = 6.25$ mm, $x_4 = 5.95$ mm, $x_5 = 5.75$ mm.

The effect of long half axis r_1 and short half axis r_2 on the AR at the maximum radiation direction with different frequencies of the proposed CP LWA is shown in Fig. 7. When r_1 increases from 6.0 to 8.1 mm, the AR at the center frequency of 10 GHz fall from 5.2 to 1.47 dB, with significant changes with different frequencies. As shown in Fig. 7(b), when the short half axis r_2 increases from 2.4 to 3.2 mm, the AR at 10 GHz increases and is less than 3 dB in the frequency range of 8.7 to 11.5 GHz. Therefore, r_1 and r_2 are selected respectively as 6.7 mm and 2.4 mm to meet the requirement of an axial ratio less than 3 dB within the HPBW range of the proposed CP LWA.

3. EXPERIMENT RESULTS AND DISCUSSION

To validate the analysis and demonstrate the antenna performance, the proposed CP LWA is fabricated and shown in Fig. 8. The far-field performances of the fabricated antenna are measured in an anechoic chamber, and the S-parameters are measured by an Agilent N5230A vector network analyzer.

Figure 9 gives the simulated and measured S-parameters of the proposed CP LWA. The measured reflection coefficient $|S_{11}|$ is -16.3 dB at center frequency of 10 GHz with the -10-dB bandwidth of 30% from 8.5 to 11.5 GHz. The simulated and measured far-field normalized right-hand circularly-polarized (RHCP) and left-hand circularly-polarized (LHCP) radiation patterns at different frequencies are shown in Figs. 10 and 11, respectively. It can be seen that the simulated antenna's RHCP main beam is scanned from $-24°$ to $+29°$, and the measured beam is scanned from $-25°$ to $+28°$ with a frequency sweep from 8.7 to 11.5 GHz. Meanwhile, the main beam for the center frequency of 10 GHz is in the broadside direction ($\theta = 0°$). The beam scanning from backward to forward is realized for

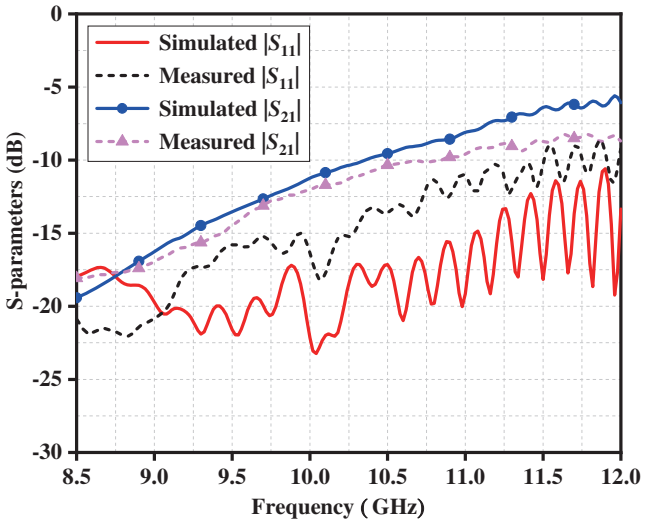

FIGURE 9. Simulated and measured S-parameters of the proposed CP LWA.

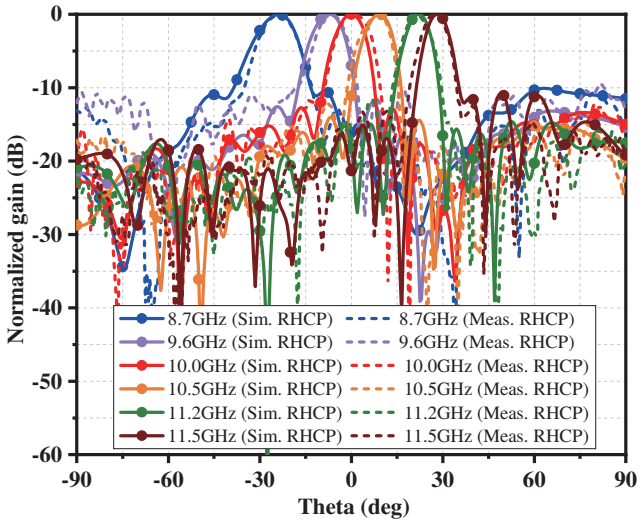

FIGURE 10. Simulated and measured normalized RHCP radiation patterns at different frequencies of the proposed CP LWA.

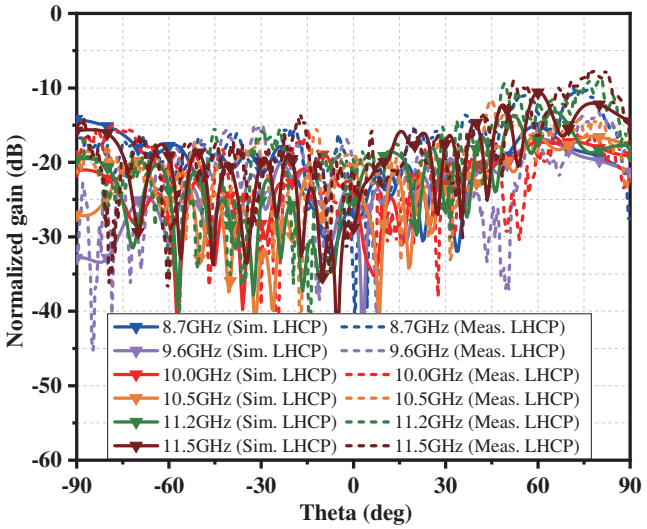

FIGURE 11. Simulated and measured normalized LHCP radiation patterns at different frequencies of the proposed CP LWA.

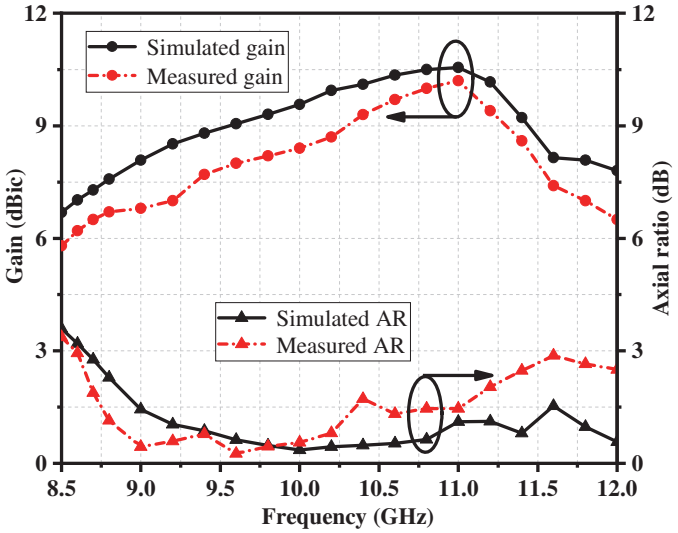

FIGURE 12. Simulated and measured gain and AR at the main beam of the proposed CP LWA.

TABLE 1. Simulated and measured radiation performance of the proposed CP LWA.

Frequency (GHz)	Beam direction (degree)		HPBW range (degree)		AR in the HPBW (dB)		Gain (dBic)	
	Sim.	Meas.	Sim.	Meas.	Sim.	Meas.	Sim.	Meas.
8.7	-24	-25	$-31 \sim -18$	$-32 \sim -19$	< 2.86	< 2.85	7.29	6.50
9.5	-9	-9	$-15 \sim -3.9$	$-14.5 \sim -4.0$	< 2.54	< 2.77	8.93	7.85
10	0	0	$-5.3 \sim +4.7$	$-5.0 \sim +5.5$	< 0.84	< 1.60	9.56	8.40
10.5	$+9$	$+8$	$+4.2 \sim +13.6$	$+3.5 \sim +12.5$	< 2.40	< 2.80	10.14	9.50
11.2	$+22$	$+21$	$+17.8 \sim +26$	$+16.5 \sim +24$	< 2.95	< 2.95	10.16	9.40
11.5	$+29$	$+28$	$+24 \sim +32$	$+23 \sim +32$	< 3.70	< 4.75	8.94	8.20

the proposed CP LWA. Besides, measured results show that the side-lobe levels below -10 dB are realized in the range of 8.7 to 11.5 GHz. Fig. 12 gives the measured gain and AR at the main beam of the proposed CP LWA. It is observed that the measured gain is more than 6.8 dBic with a peak gain of 10.35 dBic, and the AR is less than 3 dB from 8.6 to 12 GHz. Fig. 13 gives simulated and measured ARs within the HPBW at different frequencies of the proposed CP LWA. As shown in Fig. 13, the mea-

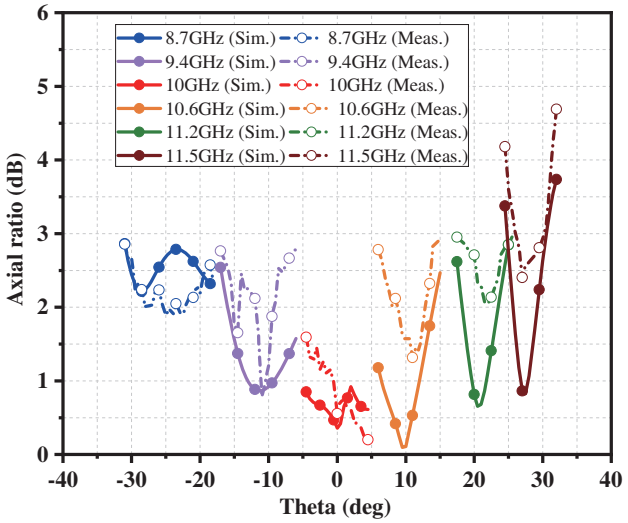

FIGURE 13. Simulated and measured AR within the HPBW at different frequencies of the proposed CP LWA.

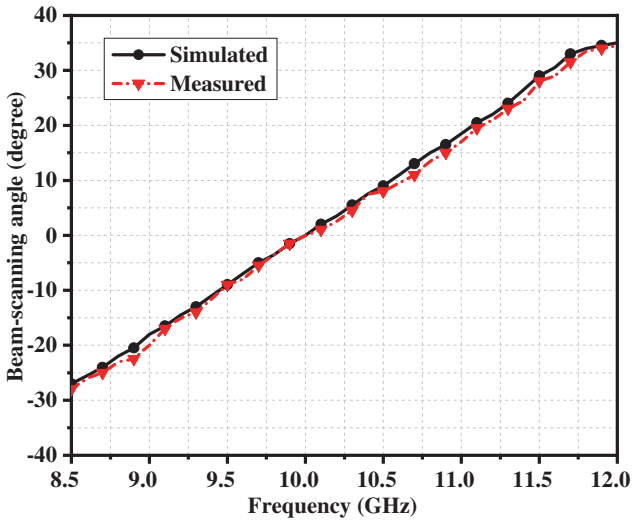

FIGURE 14. Simulated and measured main beam-scanning angle with different frequencies of the proposed CP LWA.

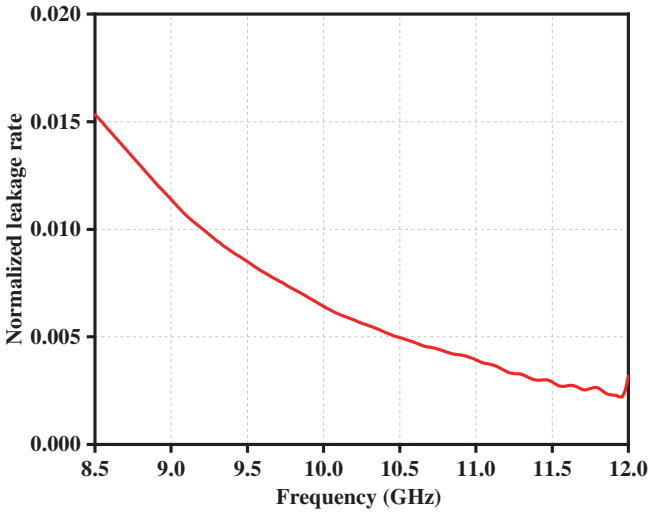

FIGURE 15. Normalized leakage rate with different frequencies of the proposed CP LWA.

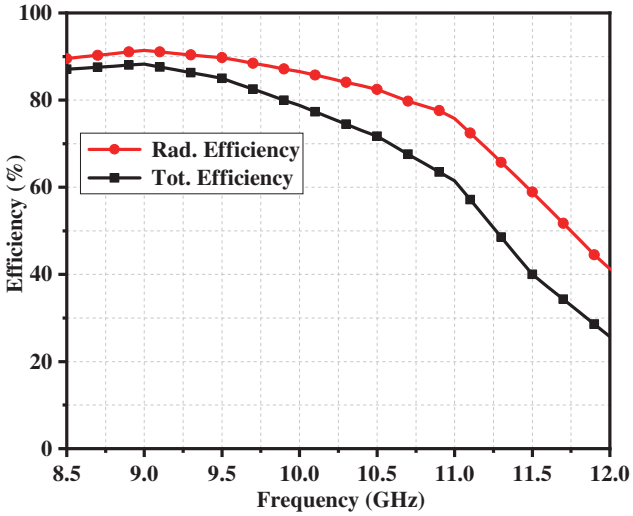

FIGURE 16. Radiation efficiency and total efficiency with different frequencies of the proposed CP LWA.

TABLE 2. Comparisons between the proposed CP LWA and the existing CP leaky-wave antennas.

Ref.	Band (GHz)	Type of Antenna	SL	SR	3-dB AR BW	Half-power beamwidth AR BW*	Gain (dBic)
[7]	7.5–11.7	Microstrip	1	$-48°$ to $+16°$	13.3%	/	15.8
[8]	12–16.5	SSPP + patch	2	$-5.0°$ to $+37°$	15%	/	9.5
[9]	11–15	SSPP + patch	2	$-32°$ to $+34°$	30.7%	/	< 15.6
[10]	8.3-9.0	SSPP + patch	2	$-26°$ to $-4.0°$	6.9%	/	11.6
[11]	7.2–8.35	Modulated SL-SSPP TL	1	$-23°$ to $-58°$	14.8%	/	8.2
[12]	5.0–7.0	SSPP + patch	1	$-6.0°$ to $+8.0°$	15%	/	10.5
[13]	9.5–9.9	Microstrip	1	$-13°$ to $+13°$	5.0%	2.8%	< 10.5
[14]	7.2–8.2	"Herringbone" array	1	$-25°$ to $+20°$	13%	13%	< 12.0
This work	**8.5–11.5**	**Slow-wave TL + patch**	**1**	$-27°$ **to** $+28°$	**27.7%**	**25.1%**	**10.35**

SL: substrate layer; SR; scanning range; TL: transmission line; BW: bandwidth; * Bandwidth for the AR less than < 3 dB within the HPBW.

sured highest AR over the major lobe HPBW is less than 3 dB from 8.7 to 11.2 GHz, and it is 1.6 dB at the center frequency of 10 GHz. The simulated and measured main beam-scanning angles with different frequencies are presented in Fig. 14. The measurement results agree well with the simulated ones.

The normalized leakage rate of the proposed CP LWA can be calculated [18]. Fig. 15 shows the normalized leakage rate with different frequencies of the proposed CP LWA. It can be seen that the normalized leakage rate varies from 0.0137 to 0.0029 at operating frequency range from 8.7 to 11.5 GHz. Fig. 16 shows the radiation efficiency and total efficiency versus frequency for the proposed CP LWA. The radiation efficiency and total efficiency at center frequency of 10 GHz are 86.54% and 78.78%, respectively.

Table 1 provides a more detailed comparison between simulated and measured radiation performances. It can be seen that the simulated beam angle is scanned from $-24°$ to $+29°$, and the measured scanning angle is from $-25°$ to $+28°$. The AR of less than 3 dB in all the HPBW ranges is satisfied for the proposed CP LWA from 8.7 to 11.2 GHz. In addition, the simulated HPBW range for the center frequency of 10 GHz is from $-5.3°$ to $+4.7°$, and the measured HPBW range is from $-5.0°$ to $+5.5°$. There are some discrepancies between simulated and measured results, which are mainly due to inaccurate values of the dielectric constant of the F4B substrates in the fabricated prototype.

Table 2 compares the proposed CP LWA with the previous existing CP LWAs. The proposed CP LWA has a wider operation bandwidth, single-layer substrate, simple structure, suitable scanning angle and gain. Furthermore, the feature that the AR within all the HPBW ranges less than 3 dB is integrated into this designed antenna, which ensures the polarization quality of circularly polarized waves.

4. CONCLUSIONS

In this paper, a novel X-band CP LWA with beam-scanning from backward to forward and AR less than 3 dB within all the HPBWs has been presented. The periodic and asymmetrical elliptical patches are loaded on both sides of slow-wave transmission line, which achieves CP radiation and wide AR bandwidth. The proposed CP LWA has realized a 3-dB AR bandwidth and the maximum gain of 27.7% and 10.35 dBic, respectively. Compared with previous leaky wave antennas [7–14], the proposed CP LWA has simple structure, wide AR bandwidth, and low AR within the HPBW, which is an excellent candidate for applications requiring CP frequency scanning features in the X-band.

ACKNOWLEDGEMENT

This work was supported by the National Natural Science Foundation of China (No. 61871417), the LiaoNing Revitalization Talents Program (No. XLYC2007024), the Fundamental Research Funds for the Central Universities (No. 3132023243), and the Open Fund of Liaoning Key Laboratory of Radio Frequency and Big Data for Intelligent Applications.

REFERENCES

[1] Jackson, D. R., C. Caloz, and T. Itoh, "Leaky-wave antennas," *Proceedings of the IEEE*, Vol. 100, No. 7, 2194–2206, Jul. 2012.

[2] Ricardi, L. J., "Communication satellite antennas," *Proceedings of the IEEE*, Vol. 65, No. 3, 356–369, 1977.

[3] Lampariello, P., F. Freeza, H. Shigesawa, M. Tsuji, and A. A. Oliner, "A versatile leaky-wave antenna based on stub-loaded rectangular waveguide: Part I — Theory," *IEEE Transactions on Antennas and Propagation*, Vol. 46, No. 7, 1032–1041, Jul. 1998.

[4] Liu, J., D. R. Jackson, and Y. Long, "Substrate integrated waveguide (SIW) leaky-wave antenna with transverse slots," *IEEE Transactions on Antennas and Propagation*, Vol. 60, No. 1, 20–29, Jan. 2012.

[5] Saghati, A. P., M. M. Mirsalehi, and M. H. Neshati, "A HMSIW circularly polarized leaky-wave antenna with backward, broadside, and forward radiation," *IEEE Antennas and Wireless Propagation Letters*, Vol. 13, 451–454, 2014.

[6] Rudramuni, K., P. K. T. Rajanna, K. Kandaswamy, B. Majumder, and Q. Zhang, "Goubau line based end-fire antenna," *International Journal of RF and Microwave Computer-aided Engineering*, Vol. 29, No. 12, Dec. 2019.

[7] Ahmad, A. and J. Mukherjee, "Microstrip leaky-wave antenna with circular polarization and broadside radiation," *IEEE Antennas and Wireless Propagation Letters*, Vol. 22, No. 9, 2265–2269, Sep. 2023.

[8] Lv, X., W. Cao, Z. Zeng, and S. Shi, "A circularly polarized frequency beam-scanning antenna fed by a microstrip spoof SPP transmission line," *IEEE Antennas and Wireless Propagation Letters*, Vol. 17, No. 7, 1329–1333, Jul. 2018.

[9] Guan, D.-F., P. You, Q. Zhang, Z.-H. Lu, S.-W. Yong, and K. Xiao, "A wide-angle and circularly polarized beam-scanning antenna based on microstrip spoof surface plasmon polariton transmission line," *IEEE Antennas and Wireless Propagation Letters*, Vol. 16, 2538–2541, 2017.

[10] Jiang, H., X. Cao, T. Liu, L. Jidi, and S. Li, "Reconfigurable leaky wave antenna with low sidelobe based on spoof surface plasmon polariton," *AEU-International Journal of Electronics and Communications*, Vol. 157, Dec. 2022.

[11] Wang, S., K. L. Chung, F. Kong, L. Du, and K. Li, "A simple circularly polarized beam-scanning antenna using modulated slotline-spoof surface plasmon polariton slow-wave transmission line," *IEEE Antennas and Wireless Propagation Letters*, Vol. 22, No. 5, 1109–1113, May 2023.

[12] Zhang, Q. L., Q. Zhang, and Y. Chen, "High-efficiency circularly polarised leaky-wave antenna fed by spoof surface plasmon polaritons," *IET Microwaves Antennas & Propagation*, Vol. 12, No. 10, 1639–1644, Aug. 2018.

[13] Ogurtsov, S. and S. Koziel, "A conformal circularly polarized series-fed microstrip antenna array design," *IEEE Transactions on Antennas and Propagation*, Vol. 68, No. 2, 873–881, Feb. 2020.

[14] Cameron, T. R., A. T. Sutinjo, and M. Okoniewski, "A circularly polarized broadside radiating "Herringbone" array design with the leaky-wave approach," *IEEE Transactions on Antennas and Propagation*, Vol. 9, 826–829, Aug. 2010.

[15] Ma, H. F., X. Shen, Q. Cheng, W. X. Jiang, and T. J. Cui, "Broadband and high-efficiency conversion from guided waves to spoof surface plasmon polaritons," *Laser & Photonics Reviews*, Vol. 8, No. 1, 146–151, Jan. 2014.

[16] Ye, L., Z. Wang, J. Zhuo, F. Han, W. Li, and Q. H. Liu, "A backfire to forward wide-angle beam steering leaky-wave antenna

based on SSPPs," *IEEE Transactions on Antennas and Propagation*, Vol. 70, No. 5, 3237–3247, May 2022.

[17] Yin, J. Y., J. Ren, Q. Zhang, H. C. Zhang, Y. Q. Liu, Y. B. Li, X. Wan, and T. J. Cui, "Frequency-controlled broad-angle beam scanning of patch array fed by spoof surface plasmon polaritons," *IEEE Transactions on Antennas and Propagation*, Vol. 64, No. 12, 5181–5189, Dec. 2016.

[18] Xu, Z., M. Wang, S. Fang, H. Liu, Z. Wang, and D. F. Sievenpiper, "Broadside radiation from chern photonic topological insulators," *IEEE Transactions on Antennas and Propagation*, Vol. 70, No. 3, 2358–2363, Mar. 2022.